**Proceedings of the ASME 2022**
**International Design Engineering Technical Conferences and**
**Computers and Information in Engineering Conference**
**IDETC/CIE 2022**
**August 14-17, 2022, St. Louis, Missouri, USA**

**DETC2022-91176**

# A VARIABLE STIFFNESS CONTINUUM PARALLEL MANIPULATOR WITH 3D PRINTED PNEUMATIC ARTIFICIAL MUSCLES

**Zhujin Jiang**

Centre for Advanced Robotics
School of Engineering and Materials Science
Queen Mary University of London
London, E1 4NS
United Kingdom
Email: z.jiang@qmul.ac.uk

**Chen Liu**

Centre for Advanced Robotics
School of Engineering and Materials Science
Queen Mary University of London
London, E1 4NS
United Kingdom
Email: chen.liu@qmul.ac.uk

**Ketao Zhang***

Centre for Advanced Robotics
School of Engineering and Materials Science
Queen Mary University of London
London, E1 4NS
United Kingdom
Email:ketao.zhang@qmul.ac.uk

## ABSTRACT

This paper presents a variable stiffness continuum parallel manipulator (VSCPM) with 3D printed pneumatic artificial muscles, which is inspired by parallel mechanisms and soft robotics. The proposed VSCPM is designed by connecting a fixed base and a moving platform with three pneumatic bellows muscles in parallel and circular distribution. A set of optimized 3D printing parameters for fabricating air tight pneumatic muscles by flexible Thermoplastic Polyurethane (TPU) filament is introduced, aiming at achieving rapid and low-cost manufacturing in comparison with other approach such as injecting silicon rubber into prefabricated molds. A prototype of the VSCPM is fabricated using the optimized 3D printing settings. The stiffness of a 3D printed bellows muscle under both positive and negative pressures is tested. The position and stiffness of the VSCPM controlled by both positive and negative pressures are also evaluated. Experimental results show that the VSCPM is capable of achieving a range of steering angle from 0° to 360° and a range of inclination angle from 0° to 45°. The stiffness of the VSCPM can also be adjusted by changing the air pressure supplied to the pneumatic artificial muscles. The novel VSCPM is compact, lightweight and soft to ensure the safe interaction with humans, which has a broad range of application such as wrist rehabilitation.

## 1 INTRODUCTION

Soft robots [1–4] have been widely investigated in recent years due to their unprecedented advantages, such as high compliance, large deformation [5], fast fabrication [6], low cost, lightweight [7] and compactness [8]. They can be actuated by variable-length tendons [9], shape-memory alloys [10] and electro-active polymers [11]. Especially, fluidic actuation [12, 13] is a new type for soft robots to deform their bodies in a continuous way and thus achieve motions with muscle-like characteristics. Fluidic elastomer actuators (FEA) are often embedded into soft bodies to achieve deformation of soft robots, and pressure used in FEA can be either pneumatic [14–16] or hydraulic [17–19]. Soft robots have a wide variety of applications from industrial to medical usages, including human-machine interaction [20], locomotion [21, 22], manipulation [23, 24], medical surgery [25], rehabilitation and wearable robotics [26].

A variety of applications require soft robots with variable stiffness to complete complex tasks, such as dexterous grippers for carrying soft/hard, light/heavy and big/small objects [27, 28], and the inflatable eversion robot for precise locomotion [29]. The variable stiffness of soft robots can be achieved by different techniques, such as electrorheological fluid with electrical signal [30], shape memory polymer with heat [31], electromagnetic suction [32] and variable stiffness material [33]. Especially,

*Address all correspondence to this author.



Copyright © 2022 by ASME

pressure-induced methods including positive pressure-inducted method [34] and negative pressure-inducted method [27] have been investigated to change the stiffness of soft robots. However, these applications use either positive pressure or negative pressure in stiffness adjustment. Few studies pay attention to the combination of both positive and negative pressures.

Soft parallel platform with artificial muscles is a typical representative of soft robots, which have similar characteristics as rigid parallel mechanism like compact structure, low inertia, and high precision [35]. The soft parallel platform has a wide range of applications, such as manipulators in medical examination [36, 37] and grasped objects [38], wrist rehabilitation [35] and robotic joints [39]. However, the soft parallel manipulator developed in [36] is actuated by hydraulic syringe pumps and only aims to bear light load, while the robotic joints presented in [39] have small workspace. To overcome the shortcomings of previous designs, this paper proposes a VSCPM with 3D printed pneumatic bellows muscles. Both positive and negative pressures are applied to adjust the position and stiffness of the VSCPM and thus to adapt to external load changes.

Further, illness like stroke may damage the central nervous system, resulting in the loss of wrist motion. Abnormal use of the wrist may also lead to wrist fractures or injuries. Thus, wrist rehabilitation training is essential for patients with wrist injuries. However, several wrist rehabilitation robots [40, 41] developed before have rigid structures with a large size, which are not flexible for patients. By contrast, inspired by parallel mechanisms and soft robots, especially the 3-SPS parallel mechanism (S means spherical joint and P means prismatic joint), the VSCPM proposed in this paper is soft, compact and lightweight, and has a wide range of potential application such as wrist rehabilitation for patients.

The contributions of this work are presented in three aspects. First, a VSCPM with 3D printed pneumatic artificial muscles is proposed. Second, the position and stiffness of the VSCPM controlled by both positive and negative pressures are evaluated. Finally, the potential application of the VSCPM for wrist rehabilitation is also demonstrated.

## 2 DESIGN AND FABRICATION OF THE VARIABLE STIFFNESS CONTINUUM PARALLEL MANIPULATOR

In this section, the design and fabrication of a variable stiffness continuum parallel manipulator with 3D printed bellows muscles shown in Fig. 1 is introduced.

### 2.1 Design of the pneumatic bellows muscle

The bellows structure fabricated by soft materials has been widely used in soft robots as it is capable of achieving a high compression/extension ratio. However, when the bellows muscle

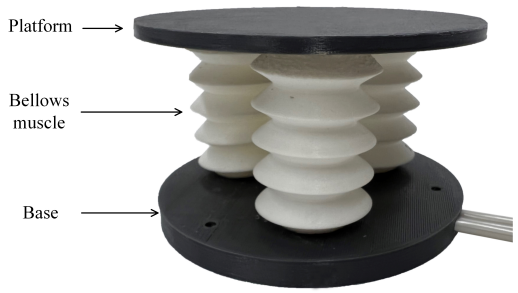


**FIGURE 1**. A NOVEL VARIABLE STIFFNESS CONTINUUM PARALLEL MANIPULATOR

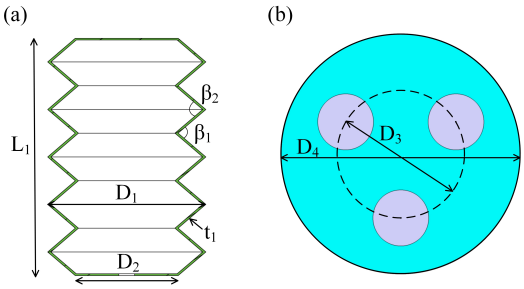


**FIGURE 2**. (A) MODEL OF THE BELLOWS MUSCLE (SECTION VIEW), (B) MODEL OF THE BASE/PLATFORM WITH THE POSITIONS OF BELLOWS MUSCLES

is manufactured by using 3D printing technique, several issues should be addressed.

The bellows muscle used as kinematic limb and actuator of the VSCPM is shown in Fig. 2(a). It is hollow and has overhangs which have a great effect on the air tightness performance of the bellows muscle. If the support for these overhangs is generated automatically, it will infill the inside of the bellows muscle and stop it from deformation. Besides, the support for overhangs is hard to design manually. Thus, support is not used to reinforce the overhangs in this work. Instead, to improve the air tightness, the printing speed is decreased to 10 mm/s, and both the angles of zigzag shape of the bellows muscle $\beta_1$ and $\beta_2$ shown in Fig. 2(a) are set to 81.2°.

Besides, the ratio between the length of the bellows muscle $L_1$ and the bottom diameter of the bellows muscle $D_2$ shown in Fig. 2(a) should be limited to 2.5. If the ratio is extremely large, the bellows muscle will be slender. When one end of the bellows muscle is attached on the build platform of a printer, the other end of the bellows muscle will become unstable, so it is difficult for a Fused Deposition Modeling (FDM) printer to deposit filament on the top of the slender bellows muscle during 3D printing, which may lead to printing failure. Thus, the length of the bellows muscle $L_1$ is set to 60 mm and the bottom diameter


Copyright © 2022 by ASME

of the bellows muscle $D_2$ is set to 26 mm in this work. Moreover, the bellows muscle is composed by 5 chambers. The outer diameter of the bellows muscle $D_1$ is 40 mm, while the thickness of the bellows muscle $t_1$ is 0.8 mm. The length of the bellows muscle in fully compressed state is 20 mm, while the length of the bellows muscle in fully extended state is 70 mm.

To perform flexible deformation without air leakage, the material selection is also essential. If the printing material is too soft, the 3D printed bellows muscle will not be able to support the moving platform of the VSCPM, and it will blow up under high pressure. By contrast, if the printing material is too stiff, the printed part will become rigid, which is hard to achieve flexible deformation. After testing several soft materials, such as Elastic 50A, Flexible 80A and NinjaFlex, TPU 95A is chosen as printing material because of its characteristics such as exceptional wear and tear resistance and rubber-like flexibility. The bellows muscle fabricated in this paper is able to withstand a pressure of 250 kPa.

### 2.2 Design of the variable stiffness continuum parallel manipulator

The proposed VSCPM is shown in Fig. 1, which consists a moving platform, a fixed base and three pneumatic bellows muscles. The bellows muscles are circularly distributed and parallel on the base for connecting the moving platform and the fixed base. The base has three channels for inserting tubes. A tube goes through the base and is inserted into each of bellows muscles for air supplying. Superglue is used to bond the tubing and the bellows muscle thus to ensure that there is not any air leakage between the tubing and the hole of the bellows muscle.

The positions of the bellows muscles influence the rotational performance and stability of the VSCPM. If the bellows muscles are close to the center of the base, the VSCPM will have a large range of rotation but low stability. By contrast, if the bellows muscles are close to the edge of the base, the VSCPM will have relatively high stability but a small range of rotation. Besides, the diameter of the platform needs to be considered. If it is too large, the edge of the platform may touch the base and prevent the platform from increasing inclination angle further. Taking these factors into account, the diameter of both the base and the platform $D_4$ is set to 120 mm and the bellows muscles are circularly distributed on the base with a diameter of 100 mm ($D_3$ in Fig. 2(b)).

The proposed VSCPM exhibits a number of advantages. First, the bellows muscles connecting the fixed base and the moving platform are 3D printed by TPU 95A material. They can be easily bent, compressed and extended. Thus, the bellows muscle can be regarded as a SPS limb and the VSCPM is a 3-SPS parallel mechanism. Compared to serial kinematic mechanism with multiple links and joints connected in series, the VSCPM has a compact structure and is capable of precise motions. Second, the bellows muscles are soft and lightweight to transmit force and motion, leading to the safe interaction with humans. Finally, the parallel manipulator is pneumatically actuated, and its stiffness and position can be adjusted by both positive and negative pressures. Unlike the parallel mechanism driven by purely positive or purely negative pressure, the stiffness and workspace of the VSCPM can be further extended.

**TABLE 1**. PRINTING SETTINGS FOR 3D PRINTED BELLOWS MUSCLES

| | |
|---|---|
| Layer Height | 0.09 mm |
| Line Width | 0.315 mm |
| Wall Thickness | 0.8 mm |
| Optimize Wall Printing Order | Yes |
| Alternate Extra Wall | Yes |
| Compensate Wall Overlaps | Yes |
| Fill Gaps Between Walls | Everywhere |
| Filter Out Tiny Gaps | Yes |
| Print Thin Walls | Yes |
| Infill Density | 100% |
| Connect Infill Lines | Yes |
| Printing Speed | 10 mm/s |
| Generate Support | No |

### 2.3 Fabrication and assembly of the variable stiffness continuum parallel manipulator

With the development of 3D printing techniques, materials with different mechanical properties are allowed to be placed at arbitrary locations within a structure. In this paper, a commercial 3D printer, the Ultimaker 3 with 0.4 mm nozzle, was used to fast print the VSCPM. The base and the platform of the VSCPM were 3D printed using polylactic acid (PLA) filament. The pneumatic bellows muscles were 3D printed using thermoplastic polyurethane (TPU) 95A filament. The settings for printing bellows muscles are essential to avoid air leaking issues and the main settings are listed in Tab. 1. Especially, the layer height is set to 0.09 mm and the print speed is set to 10 mm/s to improve the print quality. The wall thickness is 0.8 mm, which equals to the thickness of the bellows muscle modeled in CATIA V5. The line width is set to 0.315 mm as slightly reducing this value corresponding to the width of the nozzle could produce better prints. It should be noted that the wall thickness is not a multiple of the line width. This is because we have compared the trajectories


Copyright © 2022 by ASME

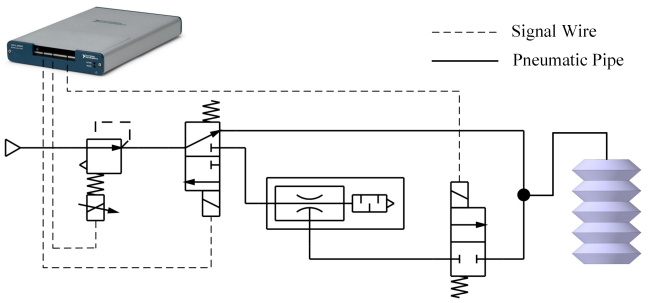


**FIGURE 3**. SCHEMATIC DIAGRAM OF THE PNEUMATIC CONTROL SYSTEM

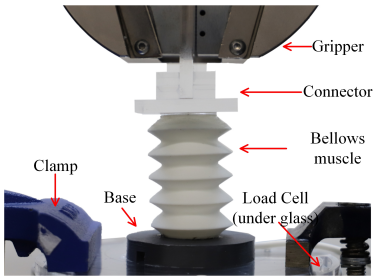


**FIGURE 4**. AXIAL STIFFNESS TEST OF THE BELLOWS MUSCLE UNDER POSITIVE AND NEGATIVE PRESSURES

of the printhead under different print settings and found that the settings of 0.315 mm line width and 0.8 mm wall thickness can ensure that the wall lines are continuous, which helps to improve the airtight performance of the bellows muscle.

After printing all components, a VSCPM was obtained by vertically attaching three bellows muscles to the base and the platform in circular distribution.

## 3 AXIAL STIFFNESS TEST OF THE BELLOWS MUSCLE

### 3.1 Experimental setup

The characteristics of the bellows muscle have an critical impact on the rotational performance and stiffness of the VSCPM. Thus, the stiffness of the bellows muscle was tested before analyzing the VSCPM.

In order to control the pressure supplied to the bellows muscles, a pneumatic control system was designed and built, as shown in Fig. 3. The data acquisition equipment, NI 6343, is used for generating control signal and receiving feedback from sensors. A pneumatic regulator, SMC ITV-212BL4, is used to control the air pressure. A 3/2-way solenoid valve is used to switch between inflation and vacuum states. A vacuum generator (ZH07DSA-06-06-06) connected to the pneumatic regulator is capable of generating negative pressure.

### 3.2 Axial stiffness test of the bellows muscle

Both positive and negative pressures have an influence on the stiffness of the bellows muscle. In order to investigate this effect, linear-force testing machine (Instron 5967) was used to exert force to the bellows muscle. The bellows muscle was fixed on the load cell of the testing machine by clamps, as shown in Fig. 4. First, positive pressure was supplied to the bellows muscle. The gripper of the testing machine moved down to compress the bellows muscle. The compression force at different lengths of the bellows muscle was measured by the testing machine. The experimental results are illustrated in Fig. 5(a). The minus sign

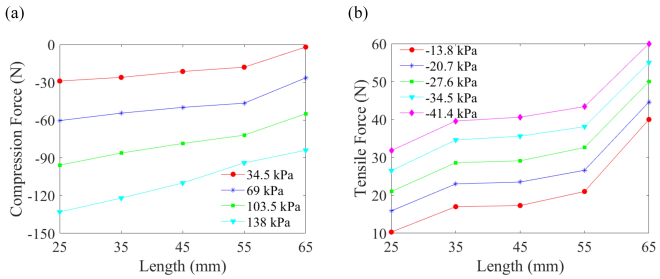


**FIGURE 5**. AXIAL STIFFNESS TEST OF THE BELLOWS MUSCLE, (A) COMPRESSION FORCE AT DIFFERENT LENGTHS, (B) TENSILE FORCE AT DIFFERENT LENGTHS

indicates the direction of the compression force points to the gripper of the testing machine.

It can be seen from Fig. 5(a) that given a certain length, the compression force significantly increases with the increase of the positive pressure. Besides, for a given positive pressure, the compression force gradually increases with the decrease of the length of the muscle. This is due to the fact that the compression of the bellows muscle increases the contact area between the bellows muscle and the connector shown in Fig. 4.

Next, negative pressure was supplied to the bellows muscle to test its effect on the stiffness of bellows muscle. The gripper of the testing machine moved up to pull the bellows muscle. The tensile force of the bellows muscle at different lengths was measured and plotted in Fig. 5(b).

Figure 5(b) shows that given a certain length, the tensile force significantly increases with the increase of the negative pressure. Besides, given a negative pressure, the tensile force gradually increases with the increase of the length of the muscle at the beginning, but sharply goes up at the end. This sharp turn results from the deformation of the TPU material.


Copyright © 2022 by ASME

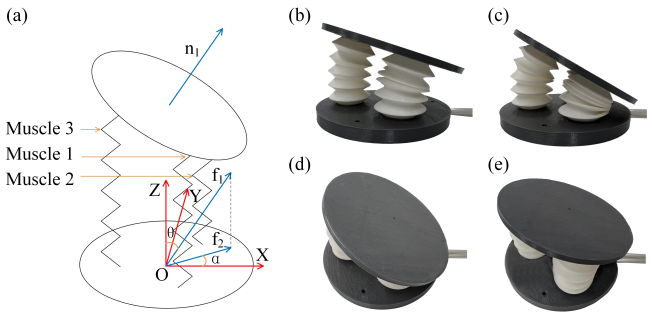


**FIGURE 6**. ROTATIONAL PERFORMANCE OF THE VSCPM

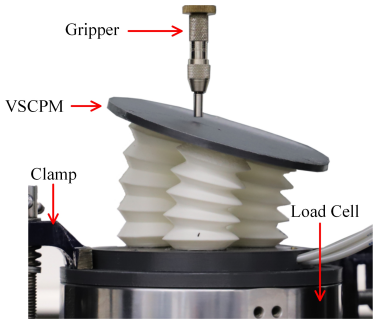


**FIGURE 7**. AXIAL STIFFNESS TEST OF THE VSCPM UNDER COMPRESSION

## 4 ROTATIONAL PERFORMANCE TEST OF THE VARIABLE STIFFNESS CONTINUUM PARALLEL MANIPULATOR

The rotational performance of the proposed VSCPM is essential for its potential application. To denote the position of the VSCPM, a global coordinate frame O-XYZ is set up at the base where the origin O is located at the center of the base, as shown in Fig. 6(a). Bellows muscle 3 is located at X-axis while bellows muscles 1 and 2 are symmetric about X-axis. The normal vector of the platform of the VSCPM is denoted by $n_1$. Vector $f_1$ is parallel to vector $n_1$ and passes the origin O. Vector $f_2$ is the projection of vector $f_1$ on the base. The inclination angle of the platform is denoted by $\theta$ which can be measured between vector $f_1$ and Z-axis, while the steering angle of the platform is denoted by $\alpha$ which can be measured between vector $f_2$ and X-axis.

The change of air pressure in the bellows muscles results in the platform of the VSCPM rotating to different positions. Figures 6(b) and 6(c) show the VSCPM in different inclination angles, while Figs. 6(d) and 6(e) show the VSCPM in different steering angles. Experiments indicate that the VSCPM presented in this work is able to achieve a range of steering angle from 0° to 360° and a range of inclination angle from 0° to 45°.

Further, the VSCPM may reach the same position under different air pressures. Table 2 gives three actuation schemes with different pressure settings for the VSCPM at each of four positions. For example, to rotate the platform of the VSCPM to the position with an inclination angle of 15° and a steering angle of 0°, we can either inflate the bellows muscle 3 with a pressure of 34 kPa, or vacuum the bellows muscles 1 and 2 with a pressure of -10.4 kPa.

## 5 AXIAL STIFFNESS TEST OF THE VARIABLE STIFFNESS CONTINUUM PARALLEL MANIPULATOR

Both positive and negative pressures have an influence on the stiffness of the VSCPM. In order to investigate this effect, The VSCPM was fixed on the load cell of the linear-force testing machine by clamps. The testing machine is able to exert force to the VSCPM and measure the displacement of the VSCPM, as shown in Fig. 7.

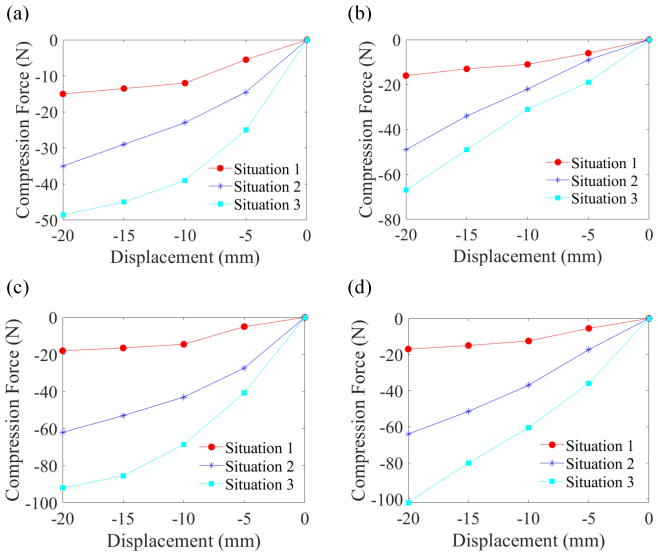


**FIGURE 8**. AXIAL STIFFNESS TEST OF THE VSCPM UNDER COMPRESSION. (A) INCLINATION ANGLE OF 15° AND STEERING ANGLE OF 0°, (B) INCLINATION ANGLE OF 30° AND STEERING ANGLE OF 0°, (C) INCLINATION ANGLE OF 15° AND STEERING ANGLE OF 60°, (D) INCLINATION ANGLE OF 30° AND STEERING ANGLE OF 60°

As the VSCPM is able to reach different inclination and steering angles, four typical positions, inclination angle of 15° and steering angle of 0°, inclination angle of 30° and steering angle of 0°, inclination angle of 15° and steering angle of 60°, inclination angle of 30° and steering angle of 60°, were chosen as the initial positions. Three actuation schemes with different pressure settings listed in Tab. 2 were selected to control the VSCPM at the same initial position. For each actuation scheme, the gripper shown in Fig. 7 was moved down to generate compression force on the platform of the VSCPM. The compression force and displacement of the VSCPM were measured and shown in Fig.


Copyright © 2022 by ASME

**TABLE 2**. ACTUATION SCHEMES FOR THE VSCPM AT DIFFERENT POSITIONS

| Positions | Inclination angle of 15° | Inclination angle of 30° | Inclination angle of 15° | Inclination angle of 30° |
|---|---|---|---|---|
| | Steering angle of 0° | Steering angle of 0° | Steering angle of 60° | Steering angle of 60° |
| Actuation scheme 1 | P1 = P2 = -10.4 kPa | P1 = P2 = -18.2 kPa | P1 = P3 = 0 | P1 = P3 = 0 |
| | P3 = 0 | P3 = 0 | P2 = -14.1 kPa | P2 = -20.3 kPa |
| Actuation scheme 2 | P1 = P2 = -6.2 kPa | P1 = P2 = -12.9 kPa | P1 = P3 = 28 kPa | P1 = P3 = 34 kPa |
| | P3 = 21 kPa | P3 = 34 kPa | P2 = -6.4 kPa | P2 = -23.2 kPa |
| Actuation scheme 3 | P1 = P2 = 0 | P1 = P2 = -10.4 kPa | P1 = P3 = 55 kPa | P1 = P3 = 69 kPa |
| | P3 = 34 kPa | P3 = 69 kPa | P2 = 0 | P2 = -21.5 kPa |

**TABLE 3**. ACTUATION SCHEMES FOR THE WRIST REHABILITATION APPLICATION OF THE VSCPM AT DIFFERENT POSITIONS

| Motions | Abduction–adduction | Supination-pronation |
|---|---|---|
| Initial Positions | Inclination angle of 0° | Inclination angle of 30° |
| | Steering angle of 0° | Steering angle of 0° |
| Actuation scheme 1 | P1 = P2 = P3 = 0 | P1 = P2 = -12.9 kPa |
| | | P3 = 34 kPa |
| Actuation scheme 2 | P1 = P2 = P3 = 20.7 kPa | P1 = P2 = -10.4 kPa |
| | | P3 = 69 kPa |
| Actuation scheme 3 | P1 = P2 = P3 = -18.2 kPa | |

8. Three curves in red, blue and cyan colors represent actuation schemes 1, 2 and 3 listed in Tab. 2, respectively.

It can be seen from Fig. 8 that the compression force increases with the increase of displacement. Besides, for a given displacement, the compression force of actuation scheme 3 is greatest in three actuation schemes. As the positive pressure of actuation scheme 3 is highest in three actuation schemes, it can be inferred that compared with the negative pressure, the positive pressure has great influence on the stiffness of the VSCPM under compression condition. The higher the positive pressure is, the greater the stiffness of the VSCPM.

## 6 WRIST REHABILITATION APPLICATION OF THE VARIABLE STIFFNESS CONTINUUM PARALLEL MANIPULATOR

To investigate the potential application of the VSCPM for wrist rehabilitation, a force-torque sensor capable of measuring the forces and torques in there directions is used to connect the handle and the VSCPM, as shown in Fig. 9(a). The coordinate frame of the force-torque sensor is denoted by O′-X′Y′Z′. The projection of the bellows muscle 3 on X′O′Y′ plane is located at X′-axis. Bellows muscles 1 and 2 are symmetric about X′O′Z′ plane.

The wrist rehabilitation application of the VSCPM can be divided into two aspects. On the one hand, when the patient holds the handle of the VSCPM with the palm, the VSCPM is controlled by adjusting the air pressure supplied to the bellows muscles to realize all the required training motions such as abduction-adduction motion and supination-pronation motion. One the other hand, the stiffness of the VSCPM can be tuned to desire values, and then the patient manually rotates the handle of the VSCPM to expected positions. As the rotational performance of the VSCPM has been validated in section 4, this section focuses on stiffness adjustment to adapt to the requirements of the patient for force training.

First, the abduction–adduction motion of the VSCPM under


Copyright © 2022 by ASME

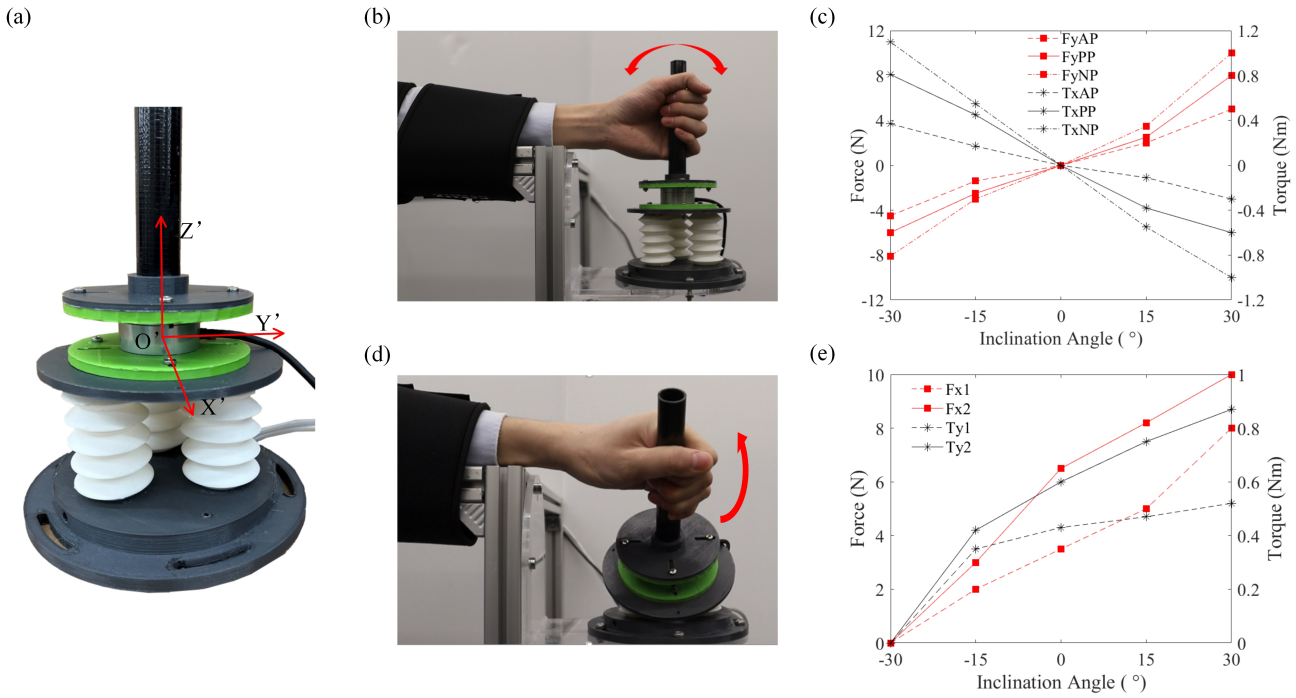


**FIGURE 9**. WRIST REHABILITATION APPLICATION OF THE VSCPM, (A) THE VSCPM WITH FORCE-TORQUE SENSOR, (B) ABDUCTION-ADDUCTION MOTION OF THE VSCPM, (C) ABDUCTION-ADDUCTION MOTION OF THE VSCPM UNDER DIFFERENT PRESSUREs, (D) SUPINATION-PRONATION MOTION OF THE VSCPM, (E) SUPINATION-PRONATION MOTION OF THE VSCPM UNDER THE COMBINATION OF POSITIVE AND NEGATIVE PRESSURES

different stiffness for wrist rehabilitation was tested by supplying equal positive or negative pressures to three bellows muscles and rotating the handle along X′-axis (Fig. 9(b)). The same motion without supplying pressure was used as a comparison, as listed in Tab. 3 (actuation schemes 1, 2 and 3 for abduction–adduction motion). The initial position of the VSCPM is at an inclination angle of 0° and a steering angle of 0°. The results are shown in Fig. 9(c) where the inclination angle $\theta$ in negative value means that the platform of the VSCPM rotates to another side. For example, the position with an inclination angle of 30° and a steering angle of 0° is the same as that with an inclination angle of −30° and a steering angle of 180°.

As shown in Fig. 9(c), the forces of the VSCPM in Y′-axis under actuation schemes 1, 2 and 3 listed in Tab. 3 are denoted by FyAP, FyPP and FyNP, respectively. The torques of the VSCPM in X′-axis under actuation schemes 1, 2 and 3 are defined as TxAP, TxPP and TxNP, respectively. It can be seen that when the VSCPM is rotated along X′-axis, the forces FyPP and FyNP are different from the FyAP, and the torques TxPP and TxNP are different from the TxAP. Thus, the stiffness of the abduction–adduction motion of the VSCPM can be adjusted by both positive and negative pressures to meet the requirements for force training of wrist rehabilitation.

Further, the supination-pronation motion of the VSCPM under different stiffness for wrist rehabilitation was tested by using two actuation schemes listed in Tab. 3 to set the VSCPM at the same initial position with an inclination angle of 30° and a steering angle of 0° , and rotating the VSCPM along Y′-axis from the initial position to the final position with an inclination angle of 30° and a steering angle of 180° (Fig. 9(d)). The experimental results are shown in Fig. 9(e).

As illustrated in Fig. 9(e), the forces of the VSCPM in X′-axis under actuation schemes 1 and 2 are denoted by Fx1 and Fx2, respectively. The torques of the VSCPM in Y′-axis under actuation schemes 1 and 2 are defined as Ty1 and Ty2, respectively. When the VSCPM is rotated along Y′-axis, the forces Fx1 and Fx2, and the torques Ty1 and Ty2 are different with each other. Thus, the stiffness of the supination-pronation motion of the VSCPM can be adjusted by the combination of positive and negative pressures to meet the requirements for force training of wrist rehabilitation.

## 7 CONCLUSIONS

This paper proposed a novel VSCPM with 3D printed pneumatic bellows muscles. The soft VSCPM was integrated by connecting the fixed base and the moving platform with three bel-


Copyright © 2022 by ASME

lows muscles in parallel and circular distribution. A prototype of the VSCPM with three pneumatic muscles was 3D fabricated using a set of optimized 3D printing parameters, and a pneumatic control system was built for inflating and vacuuming the VSCPM. The position and stiffness of the VSCPM controlled by both positive and negative pressures were evaluated. Experimental results demonstrated that the proposed VSCPM is capable of achieving a range of steering angle from $0^\circ$ to $360^\circ$ and a range of inclination angle from $0^\circ$ to $45^\circ$ via pressure control. The stiffness of the VSCPM at different positions can also be adjusted by changing the pressure supplied to the bellows muscles.

The application of the VSCPM for wrist rehabilitation was also presented. The stiffness of the VSCPM is adjusted to meet the requirements for force training of wrist rehabilitation. Comparing to the conventional robotic devices for wrist rehabilitation, the proposed VSCPM with 3D printed pneumatic muscles is compact, lightweight and soft to transmit force and motion and ensure the safe interaction with humans.

Future work will focus on implementing theoretical analysis and dynamic simulation to investigate the correlation among position, stiffness and supply pressure of the VSCPM. Control algorithms also need to be developed for adjusting the pressure supplied to the VSCPM, thereby controlling both the position and stiffness of the VSCPM at the same time.

## ACKNOWLEDGMENT

The authors thank Dr Erica Di Federico, who helped in testing the variable stiffness continuum parallel manipulator presented in this paper.

## REFERENCES

[1] Rus, D., and Tolley, M. T., 2015. "Design, fabrication and control of soft robots". *Nature,* ***521***(7553), pp. 467–475.

[2] Wang, H., Totaro, M., and Beccai, L., 2018. "Toward perceptive soft robots: Progress and challenges". *Advanced Science,* ***5***(9), p. 1800541.

[3] Schmitt, F., Piccin, O., Barbé, L., and Bayle, B., 2018. "Soft robots manufacturing: A review". *Frontiers in Robotics and AI,* ***5***, p. 84.

[4] Lipson, H., 2014. "Challenges and opportunities for design, simulation, and fabrication of soft robots". *Soft Robotics,* ***1***(1), pp. 21–27.

[5] Laschi, C., Cianchetti, M., Mazzolai, B., Margheri, L., Follador, M., and Dario, P., 2012. "Soft robot arm inspired by the octopus". *Advanced robotics,* ***26***(7), pp. 709–727.

[6] Kim, K., Agogino, A. K., Moon, D., Taneja, L., Toghyan, A., Dehghani, B., SunSpiral, V., and Agogino, A. M., 2014. "Rapid prototyping design and control of tensegrity soft robot for locomotion". In 2014 IEEE International Conference on Robotics and Biomimetics (ROBIO 2014), IEEE, pp. 7–14.

[7] Stokes, A. A., Shepherd, R. F., Morin, S. A., Ilievski, F., and Whitesides, G. M., 2014. "A hybrid combining hard and soft robots". *Soft Robotics,* ***1***(1), pp. 70–74.

[8] Watanabe, T., Yamazaki, K., and Yokokohji, Y., 2017. "Survey of robotic manipulation studies intending practical applications in real environments-object recognition, soft robot hand, and challenge program and benchmarking". *Advanced Robotics,* ***31***(19-20), pp. 1114–1132.

[9] Calisti, M., Giorelli, M., Levy, G., Mazzolai, B., Hochner, B., Laschi, C., and Dario, P., 2011. "An octopus-bioinspired solution to movement and manipulation for soft robots". *Bioinspiration & biomimetics,* ***6***(3), p. 036002.

[10] Lin, H.-T., Leisk, G. G., and Trimmer, B., 2011. "Goqbot: a caterpillar-inspired soft-bodied rolling robot". *Bioinspiration & biomimetics,* ***6***(2), p. 026007.

[11] Wallace, G. G., Teasdale, P. R., Spinks, G. M., and Kane-Maguire, L. A., 2008. *Conductive electroactive polymers: intelligent polymer systems*. CRC press.

[12] Lee, C., Kim, M., Kim, Y. J., Hong, N., Ryu, S., Kim, H. J., and Kim, S., 2017. "Soft robot review". *International Journal of Control, Automation and Systems,* ***15***(1), pp. 3–15.

[13] Pagoli, A., Chapelle, F., Corrales-Ramon, J.-A., Mezouar, Y., and Lapusta, Y., 2021. "Review of soft fluidic actuators: classification and materials modeling analysis". *Smart Materials and Structures,* ***31***(1), p. 013001.

[14] Chen, R., Zhang, C., Sun, Y., Yu, T., Shen, X.-M., Yuan, Z.-A., and Guo, J.-L., 2021. "A paper fortune teller-inspired reconfigurable soft pneumatic gripper". *Smart Materials and Structures,* ***30***(4), p. 045002.

[15] Lee, J.-G., and Rodrigue, H., 2019. "Efficiency of origami-based vacuum pneumatic artificial muscle for off-grid operation". *International Journal of Precision Engineering and Manufacturing-Green Technology,* ***6***(4), pp. 789–797.

[16] Lee, J.-G., and Rodrigue, H., 2019. "Origami-based vacuum pneumatic artificial muscles with large contraction ratios". *Soft robotics,* ***6***(1), pp. 109–117.

[17] Li, S., Vogt, D. M., Rus, D., and Wood, R. J., 2017. "Fluid-driven origami-inspired artificial muscles". *Proceedings of the National academy of Sciences,* ***114***(50), pp. 13132–13137.

[18] Katzschmann, R. K., Marchese, A. D., and Rus, D., 2016. "Hydraulic autonomous soft robotic fish for 3d swimming". In Experimental Robotics, Springer, pp. 405–420.

[19] Polygerinos, P., Wang, Z., Galloway, K. C., Wood, R. J., and Walsh, C. J., 2015. "Soft robotic glove for combined assistance and at-home rehabilitation". *Robotics and Autonomous Systems,* ***73***, pp. 135–143.

[20] Majidi, C., 2014. "Soft robotics: a perspective—current trends and prospects for the future". *Soft robotics,* ***1***(1), pp. 5–11.


Copyright © 2022 by ASME

[21] Tolley, M. T., Shepherd, R. F., Karpelson, M., Bartlett, N. W., Galloway, K. C., Wehner, M., Nunes, R., Whitesides, G. M., and Wood, R. J., 2014. "An untethered jumping soft robot". In 2014 IEEE/RSJ International Conference on Intelligent Robots and Systems, IEEE, pp. 561–566.

[22] Shepherd, R. F., Ilievski, F., Choi, W., Morin, S. A., Stokes, A. A., Mazzeo, A. D., Chen, X., Wang, M., and Whitesides, G. M., 2011. "Multigait soft robot". *Proceedings of the national academy of sciences,* ***108***(51), pp. 20400–20403.

[23] Deimel, R., and Brock, O., 2016. "A novel type of compliant and underactuated robotic hand for dexterous grasping". *The International Journal of Robotics Research,* ***35***(1-3), pp. 161–185.

[24] McMahan, W., Chitrakaran, V., Csencsits, M., Dawson, D., Walker, I. D., Jones, B. A., Pritts, M., Dienno, D., Grissom, M., and Rahn, C. D., 2006. "Field trials and testing of the octarm continuum manipulator". In Proceedings 2006 IEEE International Conference on Robotics and Automation, 2006. ICRA 2006., IEEE, pp. 2336–2341.

[25] Jiang, A., Secco, E., Wurdemann, H., Nanayakkara, T., Dasgupta, P., and Athoefer, K., 2013. "Stiffness-controllable octopus-like robot arm for minimally invasive surgery". In Workshop on New Technologies for Computer/Robot Assisted Surgery, pp. 1–2.

[26] Maeder-York, P., Clites, T., Boggs, E., Neff, R., Polygerinos, P., Holland, D., Stirling, L., Galloway, K., Wee, C., and Walsh, C., 2014. "Biologically inspired soft robot for thumb rehabilitation". *Journal of Medical Devices,* ***8***(2).

[27] Li, Y., Ren, T., Chen, Y., and Chen, M. Z., 2020. "A variable stiffness soft continuum robot based on pre-charged air, particle jamming, and origami". In 2020 IEEE International Conference on Robotics and Automation (ICRA), IEEE, pp. 5869–5875.

[28] Al Abeach, L. A., Nefti-Meziani, S., and Davis, S., 2017. "Design of a variable stiffness soft dexterous gripper". *Soft robotics,* ***4***(3), pp. 274–284.

[29] Ataka, A., Abrar, T., Putzu, F., Godaba, H., and Althoefer, K., 2020. "Model-based pose control of inflatable eversion robot with variable stiffness". *IEEE Robotics and Automation Letters,* ***5***(2), pp. 3398–3405.

[30] Tonazzini, A., Sadeghi, A., and Mazzolai, B., 2016. "Electrorheological valves for flexible fluidic actuators". *Soft Robotics,* ***3***(1), pp. 34–41.

[31] Yang, Y., Chen, Y., Li, Y., Wang, Z., and Li, Y., 2017. "Novel variable-stiffness robotic fingers with built-in position feedback". *Soft robotics,* ***4***(4), pp. 338–352.

[32] Zeng, M., Li, Y.-J., Ren, T., and Tu, Q., 2019. "Material stiffness control of compliant tools by using electromagnetic suction". *Proceedings of the Institution of Mechanical Engineers, Part C: Journal of Mechanical Engineering Science,* ***233***(13), pp. 4719–4728.

[33] Kuder, I. K., Arrieta, A. F., Raither, W. E., and Ermanni, P., 2013. "Variable stiffness material and structural concepts for morphing applications". *Progress in Aerospace Sciences,* ***63***, pp. 33–55.

[34] Godaba, H., Sajad, A., Patel, N., Althoefer, K., and Zhang, K., 2020. "A two-fingered robot gripper with variable stiffness flexure hinges based on shape morphing". In 2020 IEEE/RSJ International Conference on Intelligent Robots and Systems (IROS), IEEE, pp. 8716–8721.

[35] Wang, Y., and Xu, Q., 2021. "Design and testing of a soft parallel robot based on pneumatic artificial muscles for wrist rehabilitation". *Scientific Reports,* ***11***(1), pp. 1–11.

[36] Lindenroth, L., Soor, A., Hutchinson, J., Shafi, A., Back, J., Rhode, K., and Liu, H., 2017. "Design of a soft, parallel end-effector applied to robot-guided ultrasound interventions". In 2017 IEEE/RSJ International Conference on Intelligent Robots and Systems (IROS), IEEE, pp. 3716–3721.

[37] Lindenroth, L., Housden, R. J., Wang, S., Back, J., Rhode, K., and Liu, H., 2019. "Design and integration of a parallel, soft robotic end-effector for extracorporeal ultrasound". *IEEE Transactions on Biomedical Engineering,* ***67***(8), pp. 2215–2229.

[38] Tawk, C., Gillett, A., in het Panhuis, M., Spinks, G. M., and Alici, G., 2019. "A 3d-printed omni-purpose soft gripper". *IEEE Transactions on Robotics,* ***35***(5), pp. 1268–1275.

[39] Dong, X., Wang, Y., Liu, X., and Zhao, H., 2022. "Development of modular multi-degree-of-freedom hybrid joints and robotic flexible legs via fluidic elastomer actuators". *Smart Materials and Structures*.

[40] Squeri, V., Masia, L., Giannoni, P., Sandini, G., and Morasso, P., 2013. "Wrist rehabilitation in chronic stroke patients by means of adaptive, progressive robot-aided therapy". *IEEE transactions on neural systems and rehabilitation engineering,* ***22***(2), pp. 312–325.

[41] Krebs, H. I., Volpe, B. T., Williams, D., Celestino, J., Charles, S. K., Lynch, D., and Hogan, N., 2007. "Robot-aided neurorehabilitation: a robot for wrist rehabilitation". *IEEE transactions on neural systems and rehabilitation engineering,* ***15***(3), pp. 327–335.


Copyright © 2022 by ASME